

Effect of MgO MicroParticles on Characteristics of Microarc Oxidation Coatings Fabricated on Pure Titanium

Ping Wang*, YouTao Xiao, ZhenHui Zhou, Jun Pu, WenJie Cao, Zeyu Gong, Jie Hu

School of Materials Science and Engineering, Southwest Petroleum University, Chengdu, China

*E-mail: 818wp@163.com

Received: 13 June 2018 / Accepted: 18 October 2018 / Published: 30 November 2018

Microarc oxidation coatings were successfully fabricated on TA2 pure titanium by the microarc oxidation method in electrolyte solutions using different concentrations of MgO microparticles (0~4 g/L). The effect of MgO microparticles on the surface morphologies, composition and properties of the MAO coatings was investigated. It was observed that the concentration of MgO microparticles had a significant impact on the characteristics of the MAO coatings. With increasing concentrations of MgO microparticles, the oxidation voltage increased, and the microhardness, thickness and interface adhesion of the MAO coatings increased. The surface roughness of the MAO coatings gradually increased. MAO coatings are mainly composed of SiO₂, rutile, anatase, MgTiO₃ and MgO. The corrosion rates exhibited a trend from decreasing to increasing rates. The samples exhibited good thermal shock resistance properties.

Keywords: Microarc oxidation; MgO microparticles; Pure titanium; Characteristics

1. INTRODUCTION

Pure titanium is used in a wide variety of extreme conditions with working temperatures below 300°C [1] due to its high corrosion resistance, excellent weldability and easy processing. These conditions are typical of the aerospace and chemical industries [2,3]. However, pure titanium is prone to wear due to low surface hardness [4]. This shortcoming significantly limited the development and practical application of pure titanium. At the same time, pure titanium mainly consists of α -Ti that cannot be strengthened by heat treatment [5]. Hence, it is important to improve surface properties of pure titanium by surface treatment techniques [6,7].

Among most surface treatment technologies, microarc oxidation (MAO) is an environmentally friendly and highly efficient surface treatment technology [8]. MAO technology can form ceramic coatings in situ on the surfaces of Al, Mg, Ti and their alloys. The MAO ceramic coating can greatly

improve the surface performance of treated metals [9,10]. The influencing factors of the properties of MAO coatings mainly include current density [11], additives [12] and the electrolyte solution [13]. To further enhance the properties of MAO coatings, introducing additives into the electrolytes is a common method. Studies have shown that adding ceramic microparticles into the electrolyte solution can effectively improve the properties of MAO coatings [14,15]. For example, SiO₂ microparticles can adsorb on to MAO coatings by electrophoresis and increase the microhardness of MAO coatings [16]. ZrO₂ microparticles melted during microarc discharge can cover microchannels, thereby improving the wear resistance of MAO coatings [17]. However, to date, there have been few reports on the effect of MgO microparticles on the characteristics of pure titanium MAO coatings. This investigation aimed to produce pure titanium MAO coatings with good performance by adding MgO microparticles to the electrolytes.

In this work, MAO coatings were fabricated on pure titanium by the microarc oxidation method in a Na₂SiO₃-NaOH electrolyte solution with different concentrations of MgO microparticles (0, 1, 2, 3, 4 g/L). The oxidation voltage was recorded. The morphologies, elemental contents, element distribution and phase compositions were investigated by SEM, EDS and XRD. Coating thickness, surface hardness, interface adhesion, and corrosion rates were determined and thermal shock tests were conducted to investigate the properties of the MAO coatings.

2. MATERIAL AND METHODS

The size of the TA2 pure titanium samples used in the experiment was 1.5 mm×1.5 mm× 2 mm. The nominal components of this alloy are :Fe ≤ 0.1 wt%, O ≤ 0.07 wt%, C ≤ 0.02 wt%, N ≤ 0.02 wt%, and a balancing amount of Ti . The samples were polished with abrasive paper and degreased in hot water at 95 °C before MAO treatment. The MAO device was equipped with cooling systems that maintained the electrolyte temperature at 30 °C. The stirring device was applied to enable the MgO microparticles to be dispersed homogeneously in the electrolyte solution. In the experiment, the electrolyte solution contained 18 g/L Na₂SiO₃, 1 g/L NaOH, and 3 ml/L C₃H₈O₃. To investigate the effect of MgO microparticles on the characteristics of the MAO coatings, different concentrations of MgO (0, 1, 2, 3, 4 g/L) microparticles with sizes ≤ 150 nm (Fig. 2(a)) were added to the electrolyte solution. MAO coatings were prepared under a pulse of direct current power with a peak current density of 5A/dm², a base current density of 0, a duty cycle of 40% and a frequency of 100 Hz. The MAO treatment time was maintained for 30 min. After the treatment, the samples were sealed in hot water at 95°C and dried in air.

The oxidation voltage-time plots were recorded by computer of the MAO device (WDL 20-6). The morphologies and element contents on the surface of MAO coatings were observed by a scanning electron microscope (SEM, ZEISSEVO MA15) and an energy dispersive spectrometer (EDS, OXFORD 20). The thickness was evaluated by eddy-current thickness meter (TT230) and the microhardness of MAO coatings was characterized by a microhardness tester (HXD-2000TM/LCD) with Vickers indenter at a load of 100 g. The interface adhesion of the coating-substrate interface of the MAO coatings was evaluated by a multifunctional surface performance tester (MFT-4000) with automatic loading from 0 to 20 N and a loading rate of 30 N/min. The phase composition of the MAO coatings was investigated by

X-ray diffraction (XRD, DX-2700B) with a range of 10° to 80° and a scanning speed of $0.05^\circ/\text{s}$. The potentiodynamic polarization curve was determined to evaluate the corrosion resistance of the MAO coatings by an electrochemical workstation (Autolab PGSTAT302N) in a 3.5 wt% NaCl solution at room temperature. The polarization curve scanning rate was $1.5 \text{ mV}\cdot\text{s}^{-1}$ and the potential ranged from -0.4 V to 0.3 V . An electric furnace (SX-10-12) was used to study the thermal shocking resistance properties of MAO coatings at 300°C for 10min and then the coatings were fast cooled in 25°C water for 50 cycles. The surface charge of the MgO microparticles in the electrolyte solution was analyzed using a ZETA potential instrument (Zetaprobe).

3. RESULTS AND DISCUSSION

3.1 The oxidation voltage-time plots during MAO process

Fig. 1 shows the oxidation voltage-time plots during the MAO process with different concentrations of MgO microparticles (0~4 g/L). All the curves grew rapidly at the anodic oxidation stage and gradually stabilized at the microarc oxidation stage. It was also observed that the oxidation voltage gradually increased with increasing MgO microparticle concentration.

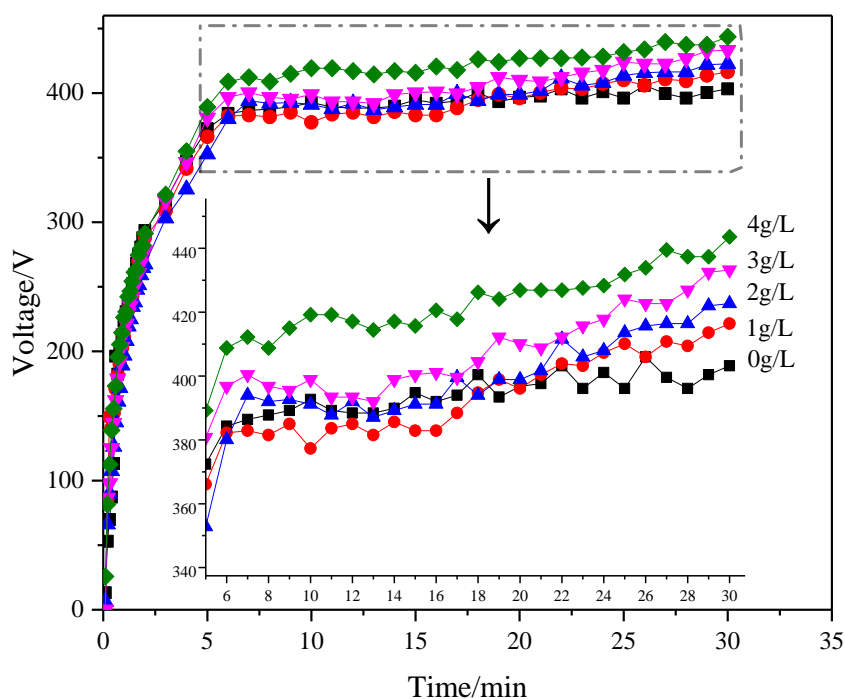


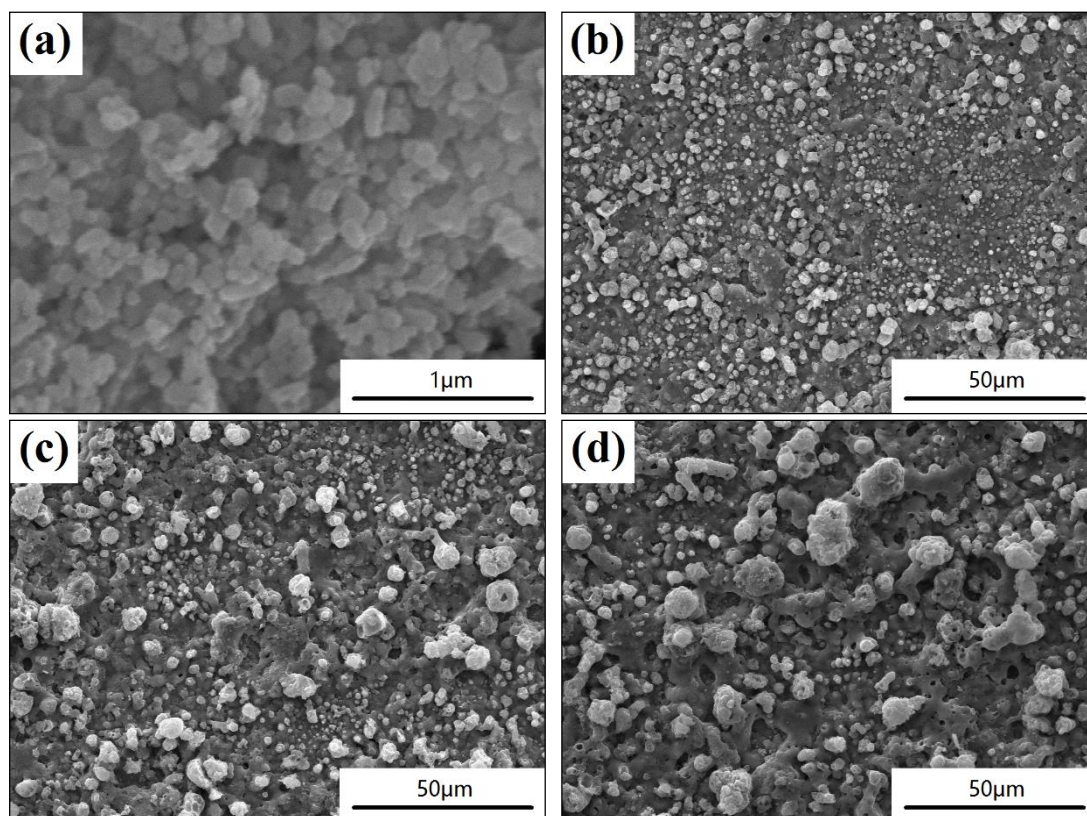
Figure 1. The oxidation voltage–time plots during the MAO process with different concentrations of MgO microparticles.

The surface charge of the MgO microparticles in the electrolyte solution was found to be -118.5 mV by the Zeta potential instrument. Li [18] noted that the addition of nano- SiO_2 particles with high dielectric strength can improve the breakdown strength of coatings. The MgO microparticles would

migrate on the surface of the sample (anode) by electrophoresis and mechanical stirring. This effect may be due to the band gaps of MgO and TiO₂ being 6.2 eV and 3.2 eV, respectively [19,20]. The dielectric strength of MgO was stronger than that of TiO₂. The MgO microparticles on the surface of the sample enhanced the dielectric strength of the MAO coatings, which led to an increase in the breakdown voltage of the MAO coatings. Hence, the oxidation voltage of the MAO coatings gradually increased with increasing MgO microparticle concentrations.

3.2 The surface morphologies of MAO coatings

Fig. 2 shows the surface morphologies of MAO coatings formed in electrolyte solutions with different concentrations of MgO microparticles (0~4 g/L). The coating surface without MgO microparticles was smooth and featured small discharge micropores and sintering discs, as shown in Fig. 2(b). From Fig. 2(c)-(g), with the increase of MgO microparticle concentration, the diameter of the micropores increased and the size of sintering discs increased.



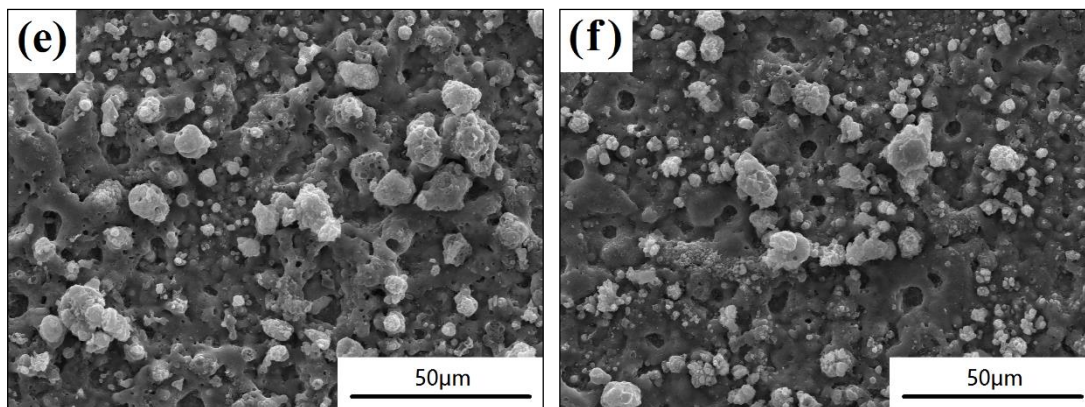


Figure 2. Surface morphologies of MAO coatings with different concentrations of MgO microparticles: (a) MgO, (b) 0 g/L, (c) 1 g/L, (d) 2 g/L, (e) 3 g/L and (f) 4 g/L

Because the high voltage could provoke strong microarc discharge and high temperature, with the increase of oxidation voltage, the microarc discharge intensified and the breakdown of MAO coatings strengthened. Then, more microareas were melted during microarc discharge. The melts solidified and formed sintering discs on the surface of the MAO coatings. Therefore, large-size sintering discs and large-diameter micropores were formed with increasing MgO microparticle concentrations. With increasing sintering disc size and micropore diameter, the surface roughness of the MAO coatings gradually increased, as shown in Fig. 3.

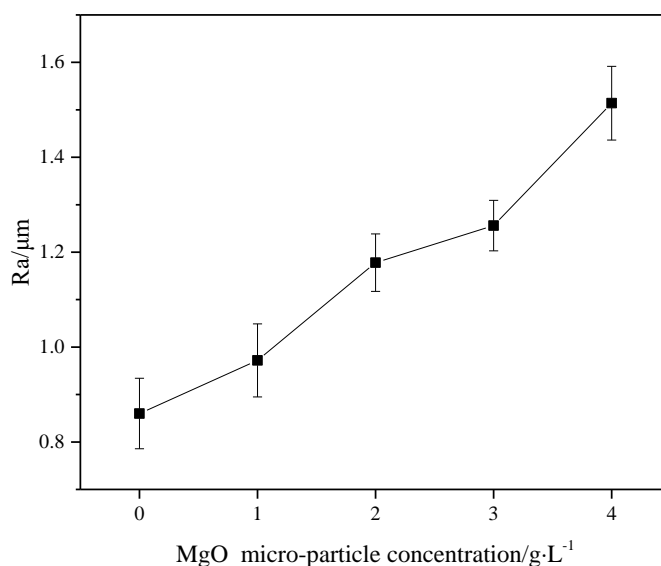


Figure 3. Surface roughness of the MAO coatings with different concentrations of MgO microparticles.

3.3 The distribution and elemental content of the surfaces of the MAO coatings

Fig. 4 reveals the distribution of Mg on the surfaces of the MAO coatings with different concentrations of MgO microparticles. At low concentrations of MgO microparticles, the distribution of Mg is relatively uniform. As the concentration of MgO microparticles increased, the distribution of Mg

gradually became enriched on the surfaces of the MAO coatings.

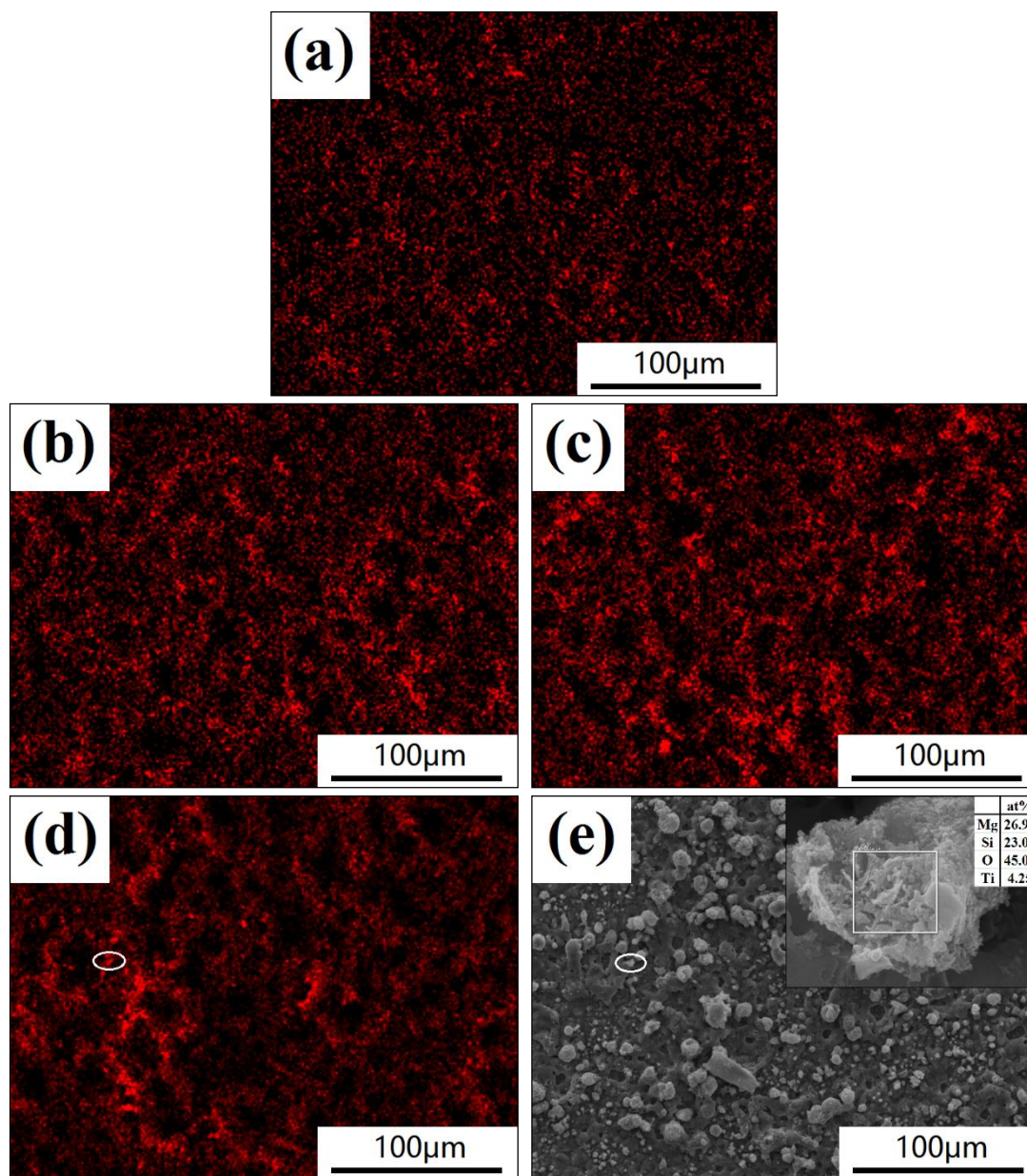
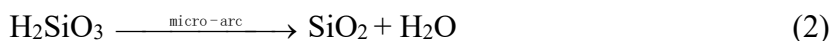
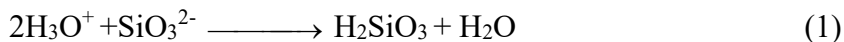


Figure 4. The distribution of Mg in MAO coatings with different concentrations of MgO microparticles: (a) 1 g/L, (b) 2 g/L, (c) 3 g/L, (d) 4 g/L, (e) SEM of 4 g/L

As seen in Fig. 4 (d)-(e), the enrichment areas of Mg mainly existed in the sintering discs and the surfaces of the sintering discs which adsorbed MgO microparticles. There are two main reasons for the enrichment of MgO microparticles on the sintering discs. On the one hand, the MgO microparticles in the solution migrated to the melt by electrophoresis and mechanical stirring and adsorbed on the surface of the sintering discs during the solidification of the melts. On the other hand, the MgO microparticles that migrated to the surface of the sample mixed with the melt and became trapped inside the melt substrate during microarc discharge. According to the SEM result, the size of the sintering discs increased with increasing concentrations of MgO microparticles. Therefore, the degree of Mg

enrichment of was greater at high concentrations of MgO microparticles.

The elemental contents (at%) on the surface of the MAO coatings are presented in Table 1. The relative amounts of Mg and Si increased gradually, while the relative amounts of Ti and O decreased. As the concentration of MgO microparticles increased, the area of Mg enrichment increased (Fig. 4 (a)-(e)), which led to more Mg on the surface of the MAO coatings. The SiO_3^{2-} in the solution could enter the MAO coatings through micropores under the effects of the electric field and generate SiO_2 during microarc discharge [21]. As a consequence, the relative amount of Si increased with increasing MgO microparticle concentration owing to the intensification of the microarc discharge. The chemical reactions of SiO_3^{2-} in the MAO coatings are as follows [21]:

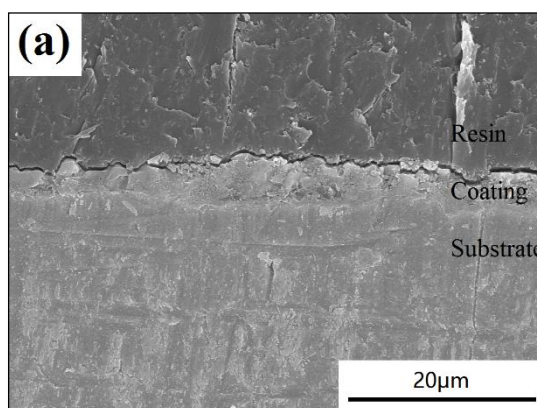


The increase in Mg and Si on the surface of the MAO coatings caused the relative amount of Ti and O to decrease.

Table 1. The elemental contents (at%) of MAO coatings with different concentrations of MgO microparticles

	Mg	Si	O	Ti
0 g/l	/	26.68	49.95	23.37
1 g/l	1.28	28.68	48.71	21.82
2 g/l	3.01	28.63	48.92	19.43
3 g/l	4.79	29.69	47.06	18.46
4 g/l	6.41	29.51	46.45	17.62

3.4 Cross-sectional images and Mg distribution of MAO coatings



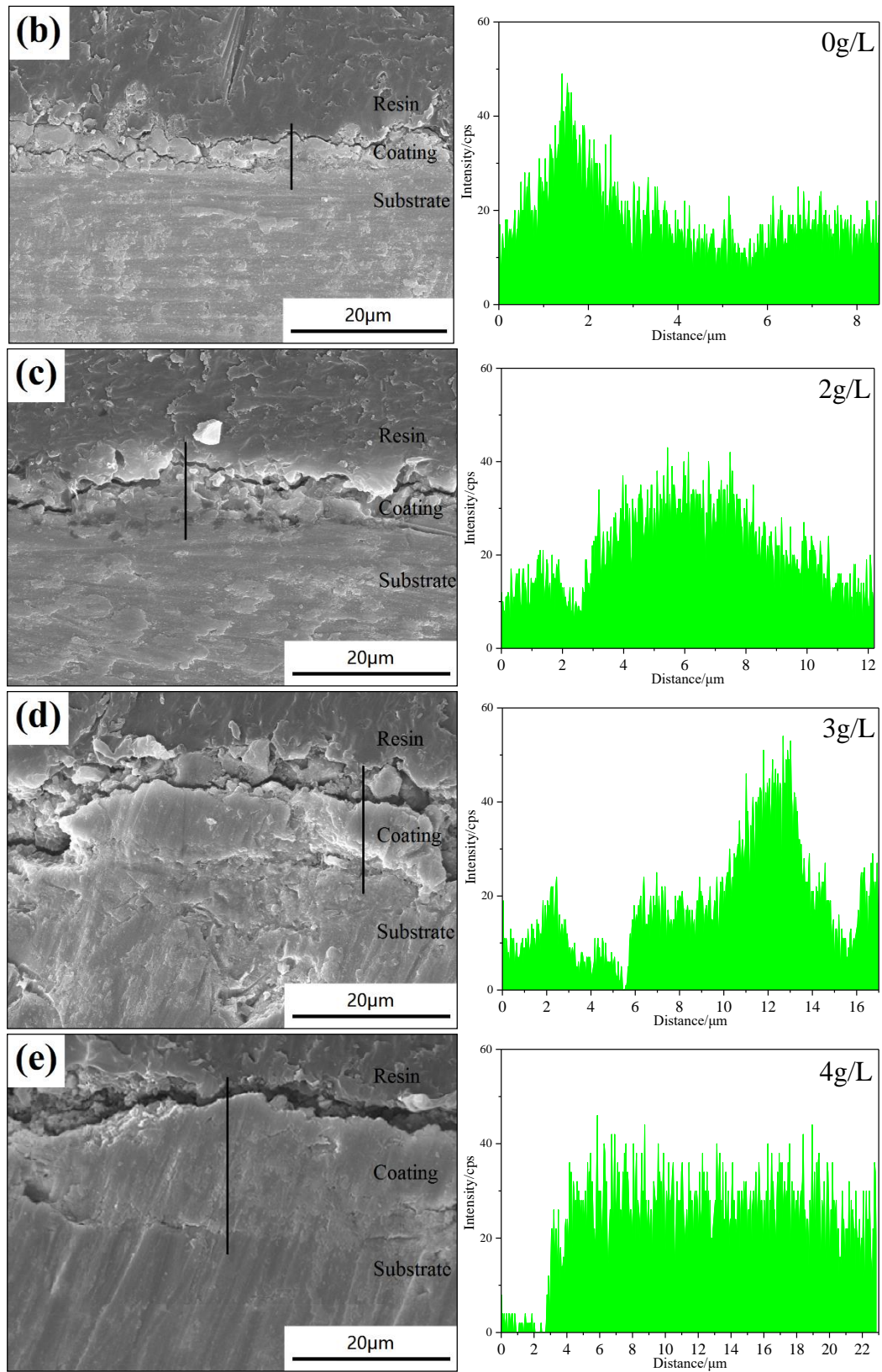


Figure 5. The cross-sectional images and Mg distribution of MAO coatings with different concentrations of MgO microparticles: (a) 0 g/L, (b) 1 g/L, (c) 2 g/L, (d) 3 g/L and (e) 4 g/L.

As revealed in Fig. 5, the thickness of the MAO coatings apparently increased. In addition, the

results of line scanning showed that Mg was mainly concentrated on the outer layer with a low concentration of MgO microparticles. With the increase in the concentration of MgO microparticles, Mg gradually diffused from the outer layer to the inner layer. From the SEM results, this effect may be explained by the fact that the diameter of the micropores on the surfaces of the MAO coatings was small at low concentrations of MgO microparticles and that the amount of MgO microparticles entering the MAO coatings was conditioned by the micropore diameter, resulting in the concentration of Mg on the outer layer. With the increase in the diameter of the micropores, the MgO microparticles easily entered the interior of the MAO coatings, and the amount of Mg in the inner layer increased.

3.5 The thickness and microhardness of MAO coatings

Fig. 6 indicates the thickness and microhardness of MAO coatings prepared with different concentrations of MgO microparticles. The thickness of the coatings was approximately 5.1, 5.7, 6.8, 9.6 and 14.5 μm . The microarc discharge could promote the growth of MAO coatings during the MAO process [22]. Therefore, the thickness of the MAO coatings increased with increasing microarc discharge. The microhardness of the MAO coatings was obviously affected by the addition of MgO microparticles in the electrolyte solution. The microhardness of the MAO coatings gradually increased as the concentration of MgO microparticles increased. This was due to the strong microarc discharge, which led to an increase in the Si content, mainly in the SiO_2 form, of the MAO coatings at high concentrations of MgO microparticles. Hence, the microhardness of the MAO coatings exhibited an upward trend with increasing concentrations of MgO microparticles.

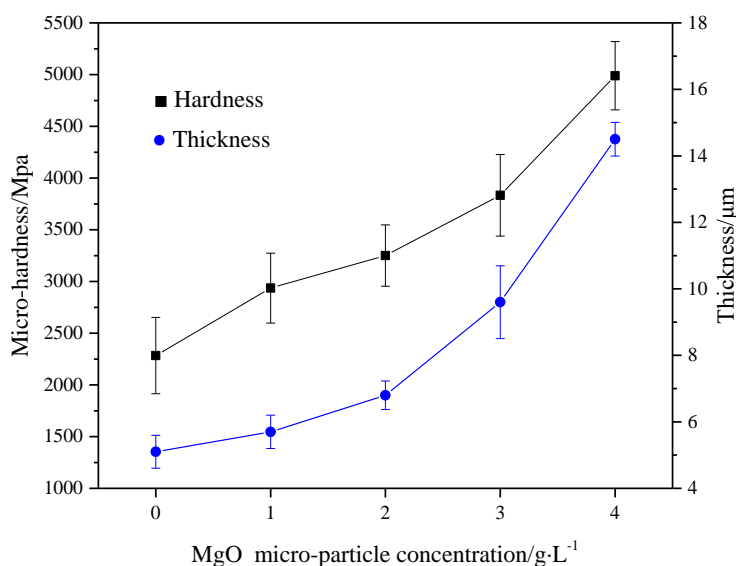


Figure 6. The thickness and microhardness of MAO coatings prepared with different MgO microparticles concentrations

3.6 The interface adhesion of the coating-substrate interface of the MAO coatings

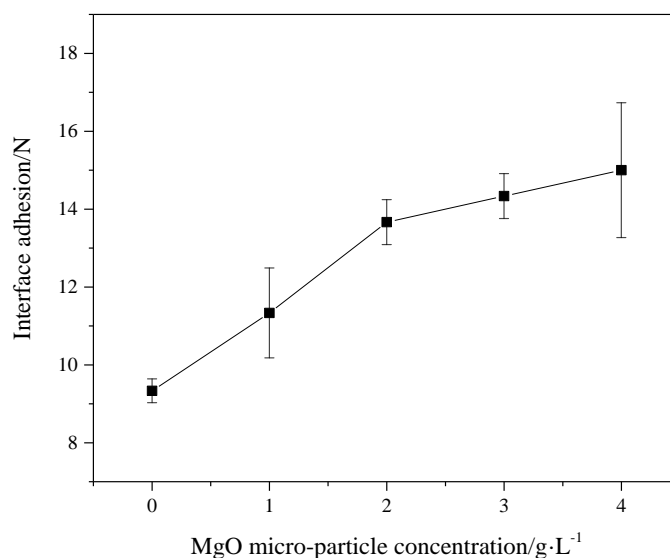


Figure 7. The interface adhesion of the coating-substrate interface of MAO coatings with different concentrations of MgO microparticles.

The interface adhesion of the coating-substrate interface of MAO coatings with different concentrations of MgO microparticles exhibits in Fig. 7. The interface adhesion of the coating-substrate interface increased with increasing MgO microparticle concentrations. A study has shown that MAO coatings exhibit metallurgical bonding with the substrate [23]. TiO₂ was mainly component at interface of coating-substrate interface [24]. High-temperature and high-pressure plasma was produced during microarc discharge [25], leading to a metallurgical effect on the MAO coatings and substrates. Accordingly, the intensification of the microarc discharge strengthened the metallurgical effect on the MAO coatings and substrates. As a result, the interface adhesion of the coating-substrate interface increased.

3.7 The phase composition of the MAO coatings

Fig. 8 shows the XRD patterns of MAO coatings with different concentrations of MgO microparticles. The XRD results reveal that MAO coatings are mainly composed of SiO₂, rutile, and anatase phases in the absence of MgO microparticles. With the addition of MgO microparticles, the MAO coatings appeared MgTiO₃ and MgO in phase. The intensity of the characteristic peaks of MgTiO₃ gradually increased with increasing concentrations of MgO microparticles. The rutile and anatase phases came from the phase transformation of TiO₂ during microarc discharge. White [26] also found that TiO₂ and MgO can be obtained by adding TiO₂ particles during the microarc oxidation process for a magnesium alloy. Research has suggested that TiO₂ and MgO can react to produce MgTiO₃ under certain conditions [27]. The phase transition process of molten TiO₂ and MgO during microarc oxidation is as follows [27]:



The reaction heat of the above formation could be calculated:

$$\Delta H_m^\ominus(298.15K) = [\Delta_f H_m(MgTiO_3, s, 298.15K)] + [(-1) \Delta_f H_m(TiO_2, s, 298.15K) + (-1) \Delta_f H_m(MgO, s, 298.15K)] = (-1497.6) \text{ KJ/mol} + [(-1) * (-994.0) \text{ KJ/mol} + (-1) * (-601.83) \text{ KJ/mol}] = 98.23 \text{ KJ/mol}$$

$$\Delta S_m^\ominus(298.15K) = [\Delta_f S_m(MgTiO_3, s, 298.15K)] + [(-1) \Delta_f S_m(TiO_2, s, 298.15K) + (-1) \Delta_f S_m(MgO, s, 298.15K)] = 111.08 \text{ J/(K}\cdot\text{mol)} + [(-1) * 50.62 \text{ J/(K}\cdot\text{mol)} + (-1) * 27 \text{ J/(K}\cdot\text{mol)}] = 33.46 \text{ J/(K}\cdot\text{mol)}$$

$$\Delta G_m^\ominus(298.15K) = \Delta H_m^\ominus(298.15K) - T \Delta S_m^\ominus(298.15K) = 98.23 \times 10^3 - 33.46 \times T$$

Obviously, when the temperature was above 2935.7 K, $\Delta G_m^\ominus(298.15 K) < 0$, indicating that this reaction could occur spontaneously. During the microarc oxidation process, the temperature of discharge zone can reach $10^3 \sim 10^4$ K in a short time [28]. It was obvious that TiO_2 reacted with MgO easily to form $MgTiO_3$ during the microarc oxidation process.

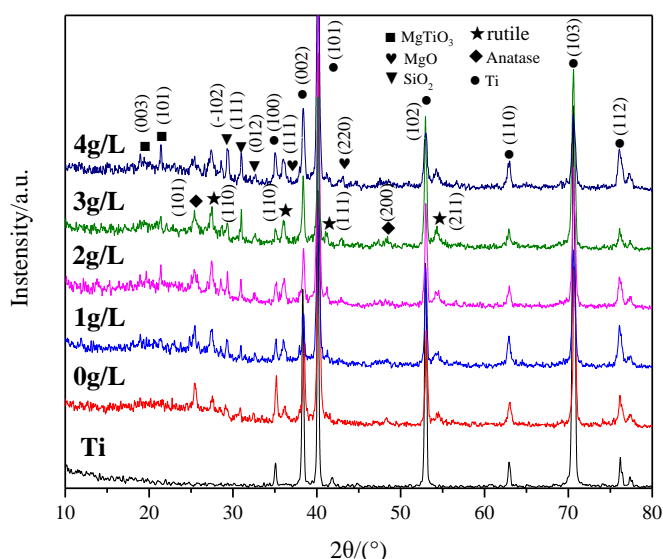


Figure 8. The XRD patterns of MAO coatings prepared with different MgO microparticles concentrations

3.8 The corrosion rates of MAO coatings

Fig. 9 displays the potentiodynamic polarization curves of MAO coatings in 3.5 wt% NaCl solution with different concentrations of MgO microparticles. According to the Stern-Geary equation [10], the corrosion current density i_{corr} was calculated as follows:

$$i_{corr} = \frac{\beta_\alpha \times \beta_c}{\beta_\alpha + \beta_c} \times \frac{1}{R_p} \tag{4}$$

Then, according to Faraday’s law, where N is equivalent weight and ρ is density:

$$V_{corr}(\text{mil}\cdot\text{year}^{-1}) = \frac{i_{corr}(\text{A}\cdot\text{cm}^{-2}) \times N(\text{g}) \times 393.7(\text{mil}\cdot\text{cm}^{-2}) / \rho(\text{g}\cdot\text{cm}^{-3}) \times 365 \times 24 \times 3600(\text{m}\cdot\text{year}^{-1})}{96500(\text{C}\cdot\text{mol}^{-1})} \tag{5}$$

$$V_{corr}(\text{mm/a}) = \frac{V_{corr}(\text{mil}\cdot\text{year}^{-1})}{39.37(\text{mil}\cdot\text{mm}^{-1})} \tag{6}$$

The fitted corrosion rates of the curves are 4.955×10^{-3} , 4.368×10^{-3} , 2.648×10^{-3} , 3.996×10^{-3} , and 4.748×10^{-3} mm/a and are listed in Table. 2. The corrosion rate was determined by the thickness and morphologies of the coatings. At low concentrations of MgO microparticles, the diameter of the micropores was small and had little influence on the corrosion resistance of the MAO coatings. The increase in the thickness of the MAO coatings could prevent the transfer of Cl^- to the substrate in the corrosion process. Hence, the corrosion rate decreased with increasing thickness from 0 g/L to 2 g/L. Although the thickness of the MAO coatings increased with the increase in the concentration of MgO microparticles, the diameter of the micropores also obviously increased with the concentration of MgO microparticles from 2 g/L to 4 g/L. In this time, the Cl^- could reach the substrate easily through the large diameter of the micropores. Therefore, the corrosion rate increased from 2 g/L to 4 g/L.

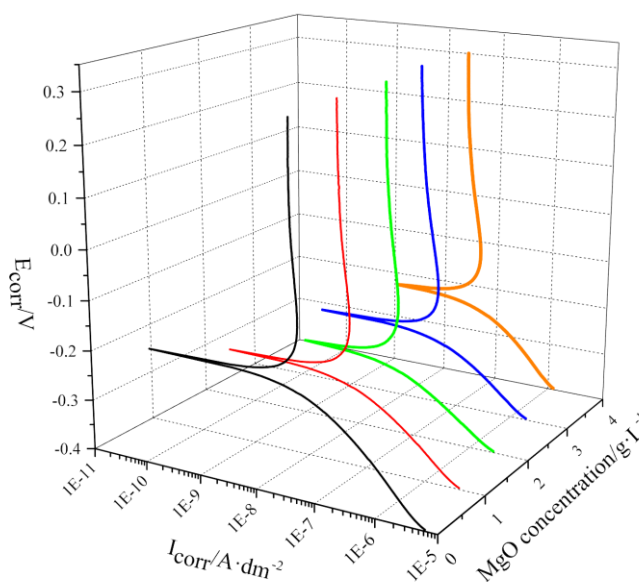


Figure 9. The potentiodynamic polarization curves for MAO coatings with different concentrations of MgO microparticles.

Table 2. The fitted corrosion rates for the MAO coatings

concentration/(g/L)	E _{corr} /V	I _{corr} /(A/cm ²)	Corrosion rate/(mm/a)
0	-0.171	8.021×10^{-8}	4.955×10^{-3}
1	-0.219	7.064×10^{-8}	4.368×10^{-3}
2	-0.243	4.283×10^{-8}	2.648×10^{-3}
3	-0.246	6.463×10^{-8}	3.996×10^{-3}
4	-0.226	7.778×10^{-8}	4.748×10^{-3}

3.9 Thermal shock test of MAO coating

Fig. 10 shows the surface morphologies of the MAO coating at 3 g/L under different

magnifications (2000 times and 7000 times) after the thermal shock tests. Comparing the surface morphologies before (Fig. 2(e)) and after (Fig. 10(a)) the thermal shock test, it can be seen that the surface morphologies of the MAO coating had changed little. Fig. 10(b) shows a microcrack on the surface of the MAO coating. The thermal expansion coefficient of Ti is $8.6 \times 10^{-6} \text{ } ^\circ\text{C}^{-1}$, but the coefficient for TiO_2 is $8.3 \times 10^{-6} \text{ } ^\circ\text{C}^{-1}$ [29]. Thermal stress leads to cracks during the thermal shock test process. However, the difference in the thermal expansion coefficients of Ti and TiO_2 was small, causing low thermal stress. Therefore, the microcrack was very tiny in Fig. 10(b). At the same time, the small difference in the thermal expansion coefficients between Ti and TiO_2 also ensured good thermal shock resistance in the MAO coatings.

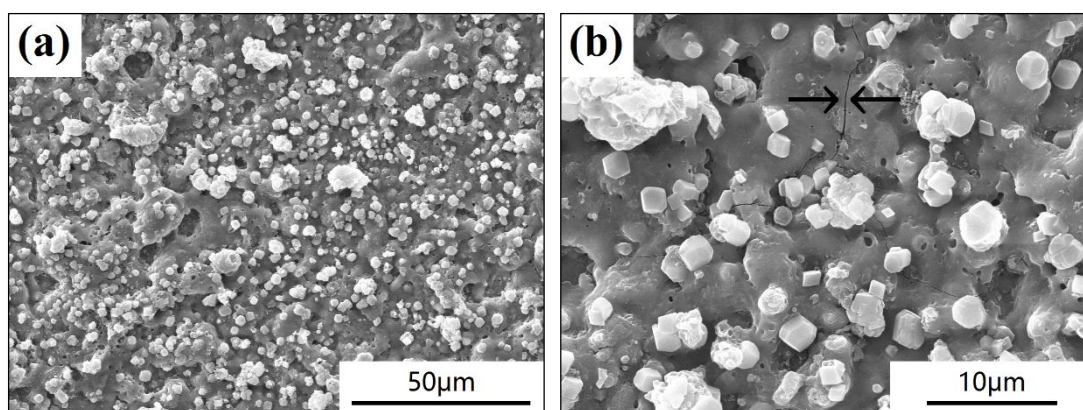


Figure 10. Surface morphologies of MAO coating at 3.0 g/L after the thermal shock tests: (a) 2000 times, (b) 7000 times

4. CONCLUSIONS

MAO coatings were successfully fabricated on pure titanium by the microarc oxidation method in electrolyte solutions with different concentrations of MgO microparticles. MgO microparticles with a negative surface charge migrated to the surface of the sample by electrophoresis and mechanical stirring, raising the oxidation voltage. The high oxidation voltage enhanced the microarc discharge. Consequently, the growth of MAO coatings was promoted and the molten microareas increased. MAO coatings are mainly composed of SiO_2 , rutile, anatase, MgTiO_3 and MgO. The EDS results showed that the amount of Mg on the surface of the MAO coatings increased gradually and mainly gathered in the sintering discs. The microhardness and interface adhesion of the coating-substrate interface of the MAO coatings increased with increasing concentrations of MgO microparticles. The corrosion rates exhibited a trend from decreasing to increasing due to the combined effects of thickness and the diameter of micropores on the MAO coatings. Despite the presence of a tiny microcrack on the surface, the thermal shock test indicated that the MAO coatings have good thermal shock resistance properties. In summary, the MAO coatings had the best comprehensive properties when the MgO microparticle concentration was 2 g/L.

References

1. S. Venugopal, P. Venugopal, S.L. Mannan, *J. Mater. Process. Tech.* 202 (2008) 201.
2. Z.B. Wang, H.X. Hu, Y.G. Zheng, *Electrochim. Acta.* 170 (2015) 300.
3. N. Sridharan, P. Wolcott, M. Dapino and S.S. Babu, *Scripta. Mater.* 117 (2016) 1.
4. H. Attar, K.G. Prashanth, A.K. Chaubey, M. Calin, L.C. Zhang, S. Scudino and J. Eckert, *Mater. Lett.* 142 (2015) 38.
5. N. Poondla, T.S. Srivatsan, A. Patnaik and M. Petraroli, *J. Alloy. Compd.* 486 (2009) 162.
6. S.J. Dai, Y.T. Zhu, Z.W. Huang, *Vacuum.*, 125 (2016) 215.
7. D. Prando, A. Brenna, F.M. Bolzoni, M.V. Diamanti, M. Pedferri and M. Ormellese, *J. Appl. Biomater. Func.* 15 (2017) 19.
8. L.J. Zhu, Z.X. Guo, Y.F. Zhang, Z.L. Li and M.L. Sui, *Electrochim. Acta.* 208 (2016) 296.
9. S. Hariprasad, M. Ashfaq, T. Arunnellaiappan, M. Harilal, N. Rameshbabu, *Surf. Coat. Tech.* 292 (2016) 20.
10. P. Wang, T. Wu, Y.T. Xiao, L. Zhang, J. Pu, W.J. Cao and X.M. Zhong, *Vacuum.* 142 (2017) 21.
11. R.H.U. Khan, A. Yerokhin, X. Li and H. Dong, A. Matthews, *Surf. Coat. Tech.* 205 (2010) 1679.
12. D. Zhao, Y. Lu, X. Zeng, Z. Wang, S.G. Liu and T. Wang, *Surf. Eng.* 33 (2017) 796.
13. J. Liang, P.B. Srinivasan, C. Blawert, M. Stormer and W. Dietzel, *Electrochim. Acta.* 54 (2009) 3842.
14. X.P. Lu, M. Mohedano, C. Blawert, E. Matykina, R. Arrabal, K.U. Kainer and M.L. Zheludkevich, *Surf. Coat. Tech.* 307 (2016) 1165.
15. M. Shokouhfar, S.R. Allahkaram, *Surf. Coat. Tech.* 291 (2016) 396.
16. X.P. Lu, C. Blawert, M.L. Zheludkevich and K.U. Kainer, *Corros. Sci.* 101 (2015) 201.
17. H. Li, Y. Sun, J. Zhang, *Appl. Surf. Sci.* 342 (2015) 183.
18. F. Li, M. Yao, Z. Su, J.W. Chen, Y. Peng, Q.X. Li and X. Li, *CERAM. INT.* 43 (2017) 349.
19. H. K. Yu, *Thin. Solid. Films.* 653 (2018) 57.
20. A. Esteves, L. C. A. Oliveira, T. C. Ramalho, M. Goncalves, A. S. Anastacio and H. W. P. Carvalho, *Catal. Commun.* 10 (2008) 330.
21. S. Moon, Y. Jeong, *Corros. Sci.* 51 (2009) 1506.
22. S. Durdu, M. Usta, *Appl. Surf. Sci.* 261 (2012) 774.
23. F. Xiao, H. Chen, J. Miao and J. Du, *Int. J. Mod. Phys.B.* 31(2017) 16.
24. M.H. Hong, D.H. Lee, K.M. Kim and Y.K. Lee, *Thin. Solid. Films.* 519 (2011) 7065.
25. Y.M. Wang, L.X. Guo, J.H. Ouyang, Y. Zhou and D.C. Jia, *Appl. Surf. Sci.* 255 (2009) 6875.
26. L. White, Y. Koo, Y. Yun and J. Sankar, *J. Nanomater.* 2013(2013)11.
27. I. Shindo, *J. Cryst. Growth.* 50 (1980) 839.
28. A. L. Yerokhin, X. Nie, A. Leyland and A. Matthews, *Surf. Coat. Tech.* 130 (2000) 195.
29. S.S. Jiang, K.F. Zhang, *Mater. Design.* 30 (2009) 3904.